can be estimated from the data in Fig. 3. The flux of electrons from the various substrates under a common flux of photons is different. We have estimated the relative intensities of electrons from the substrates by integrating (*16, 17*) the XPS spectra in Fig. 3 over the kinetic energy (KE) range from 387 to 1487 eV. We are limited by the electrostatic analyzer on the XPS to quantitation of electrons of KE $\gtrsim$ 400 eV, and there may be systematic errors in estimating the relative intensities of electrons in the range of energies that are most damaging ($\sim$50 eV) from the observed yield of electrons of energies >400 eV (*17, 18*). In Fig. 4B, we plot the intensity of F(1*s*) from the various substrates versus the number of electrons to which the SAM was exposed. In order to generate similar doses of electrons, we exposed the samples containing thicker overlayers of Si to the x-ray beam longer than those having thinner overlayers. The profiles in Fig. 4B are remarkably similar (especially given that the substrates had different lengths of exposure to the x-ray beam) and suggest that the primary and secondary electrons are much more important in the damage process than are the x-ray photons. We believe the deviations present are primarily due to difficulties in maintaining a constant photon flux.

Although the data do not determine whether electrons are solely responsible for causing damage, they are, however, consistent with the finding that primary and secondary electrons are responsible for most (and maybe all) of the damage to a representative organic system upon irradiation with x-rays.

REFERENCES AND NOTES

1. D. R. Wheeler and S. V. Pepper, *J. Vac. Sci. Technol.* **20**, 226 (1982); C. P. Buchwalter and G. Czornyji, *ibid. A* **8**, 781 (1990).
2. W. M. Moreau, *Semiconductor Lithography: Principles, Practices and Materials* (Plenum, New York, 1987), pp. 104–111.
3. W. Schnabel and H. Sotobayashi, *Prog. Polym. Sci.* **9**, 297 (1983).
4. For example, the penetration depth of x-rays (KE $\sim$2 keV) into organic materials is of the order of micrometers; of electrons, it is of the order of $\sim$100 Å [M. P. Seah, in *Practical Surface Analysis*, D. Briggs and M. P. Seah, Eds. (Wiley, Chichester, 1983), chap. 5]. In our experiment, we estimate the flux of x-ray photons experienced by the CF_3CO_2– group to be more than $\sim$100 times greater than the flux of electrons.
5. C. J. Powell and M. P. Seah, *J. Vac. Sci. Technol. A* **8**, 735 (1990).
6. C. D. Bain, thesis, Harvard University (1988).
7. R. G. Nuzzo and D. L. Allara, *J. Am. Chem. Soc.* **105**, 4481 (1983); C. D. Bain and G. M. Whitesides, *Angew. Chem. Int. Ed. Engl.* **101**, 522 (1989), and references therein; G. M. Whitesides and P. E. Laibinis, *Langmuir* **6**, 87 (1990), and references therein.
8. S. R. Wasserman, Y.-T. Tao, G. M. Whitesides, *Langmuir* **5**, 1074 (1989).
9. A. Ulman, *An Introduction to Ultrathin Organic Films* (Academic Press, Boston, 1991), pp. 245–279.
10. The "universal" curve (Fig. 3, inset) relates the inelastic mean free path of an electron, λ (the distance required to reduce the probability an electron escaping to 1/*e*) through a material to the kinetic energy of the electron [M. P. Seah and W. A. Dench, *Surf. Interface Anal.* **1**, 2 (1979)].
11. J. H. Scofield, *J. Electron Spectrosc. Relat. Phenom.* **8**, 129 (1976).
12. L. C. Feldman and J. W. Mayer, *Fundamentals of Surface and Thin Film Analysis* (Elsevier Science, New York, 1986), chaps. 2 and 3.
13. The RBS spectra were analyzed with Spectrum Analysis (SA), a PC version of the TEK program for RBS analysis developed at Oak Ridge National Laboratory. SA was written by P. M. Smith (Division of Applied Sciences, Harvard University, Cambridge, MA, 1989).
14. We tested the presence of Au at the surface of the Si/Cr/Au/Si substrates by immersing the Si-coated Au substrates in a 1 mM ethanolic solution of a F-containing alkanethiol [$CF_3CF_2CH_2O(CH_2)_{11}SH$] overnight. Thiols react with soft metal–metal oxides, such as Au, but do not react with hard metal–metal oxides, such as Al_2O_3 or SiO_2 [P. E. Laibinis, J. J. Hickman, M. S. Wrighton, G. M. Whitesides, *Science* **245**, 845 (1989); P. E. Laibinis and G. M. Whitesides, unpublished results]. No F was detected on any substrate exposing Si by XPS, suggesting that the Si-coated Au substrates reveal no (or very little) Au at their surface. We estimate that we would have detected 0.1% of a monolayer of the fluorinated thiolate.
15. We have estimated that the procedure used to derivatize Si yields $\sim$80% of the number of CF_3CO_2 groups as the procedure used to derivatize Au (*8*).
16. In estimating the relative flux of electrons from the various substrates, the spectra (Fig. 3) were corrected for differences in the efficiency of the electrostatic analyzer with the KE of the electron. The effect of this correction on the relative electron flux is small (<2%).
17. We have also analyzed the XPS spectra incorporating differences in the likelihood of an electron to interact with the SAM (estimated as 1/λ) and find that the correction would be small (≤3%); the direction of this correction is opposite that due to detector inefficiencies (*16*).
18. M. P. Seah and G. C. Smith, *Surf. Interface Anal.* **15**, 751 (1990).
19. Supported in part by the Office of Naval Research, the Defense Advanced Research Projects Agency, and the National Science Foundation (grant CHE-88-12709). XPS and RBS spectra were obtained with instrumental facilities purchased under the Defense Advanced Research Projects Agency and University Research Initiative Program and maintained by the Harvard University Materials Research Laboratory. We thank J. F. Chervinsky and P. M. Smith for help in characterizing the substrates by RBS, J. P. Folkers for supplying the $H_2C{=}CH(CH_2)_9SiCl_3$, C. D. Bain for discussions and suggestions, and S. M. Bonser, J. P. Folkers, and J. P. Mathias for critical readings of this manuscript.

29 May 1991; accepted 30 August 1991

Scanning Tunneling Microscopy of Galena (100) Surface Oxidation and Sorption of Aqueous Gold

CARRICK M. EGGLESTON* AND MICHAEL F. HOCHELLA, JR.

Scanning tunneling microscopy was used to characterize the growth of oxidized areas on galena (100) surfaces and the formation of gold islands by the reductive adsorption of $AuCl_4^-$ from aqueous solution. The gold islands and galena substrate were distinguished by atomic resolution imaging and tunneling spectroscopy. Oxidized areas on galena have [110]-trending boundaries; gold islands elongate along [110] directions. However, there are no obvious structural registry considerations that would lead to elongation of gold islands in a [110] direction. Instead, it is probable that a direct coupling of gold reduction and sulfide surface oxidation controls the initial formation of gold islands. Gold islands grow less quickly on preoxidized galena surfaces and show no preferred direction of growth.

REDOX REACTIONS AT THE SULFIDE-water interface are thought to play an important role in the formation of certain sulfide-hosted heavy metal ore deposits (*1, 2*). For example, recent studies have established a clear connection between the adsorption and reduction of aqueous Au by sulfide surfaces and concomitant sulfide oxidation, although the role of the semiconducting sulfide (whether *n*- or *p*-type) and the exact mechanisms remain uncertain (*2*). Our goal is to understand the chemical and structural mechanisms that drive these sorption-reduction reactions at mineral-water interfaces. We have used scanning tunneling microscopy (STM) and tunneling spectroscopy to examine atomic level structural controls on the oxidation of galena (PbS) in air and aqueous solutions and to examine relations between surface oxidation and the sorption-reduction of Au from Au(III) chloride–containing aqueous solutions (*3*). Although the pyrite–Au(I) bisulfide system is more relevant to sediment-hosted epithermal Au deposits, the galena–Au(III) chloride system was chosen for this study because it is experimentally simple (experiments can be performed under ambient conditions) and it is relatively well characterized (*2*). In addition, galena has perfect [100] cleavage and its surface electronic characteristics and bonding structure have been studied (*4*). Low-energy electron diffraction

---

C. M. Eggleston, Department of Applied Earth Sciences, Stanford University, Stanford, CA 94305.
M. F. Hochella, Jr., Department of Geology, Stanford University, Stanford, CA 94305.

*Present address: Swiss Federal Institute for Water Resources and Water Pollution Control (EAWAG), CH-8600 Dubendorf, Switzerland.

(LEED) shows that the (100) surface, exposed by fracturing in air, does not reconstruct (*5*). STM studies of the galena (100) surface have included discussions of defect structures (*6–8*) and image interpretation (*9*).

Because galena oxidizes slowly in air (*10*), we were able to cleave it under ambient conditions and then both induce and observe oxidation with the STM. A tip bias of −200 mV in air was used for this purpose. A fresh galena (100) surface imaged within 3 min of cleavage shows dominant spots that correspond to S sites (Fig. 1A) (*9*). Dark areas are roughly rectangular, with edges parallel to [110] and equivalent directions. In the time it took to complete the next scan (33 s), the dark areas grew and coalesced (Fig. 1B). We believe that the dark patches in Fig. 1 form as a result of the oxidation of surface sulfide sites. The rate of the observed reaction is in rough agreement with the results of voltammetry measurements for aqueous galena oxidation (*11*) and is too slow to be the result of the chemisorption of O-containing species to Pb sites as characterized by photoelectron spectroscopy (PES) (*10, 12*). Furthermore, the oxidation of surface sulfide will most likely alter the local bonding and electronic structure so as to reduce the tunneling current over oxidized sites (lead sulfate is an insulator); this process results in apparent topographic lows in STM images. However, regardless of the area imaged on the sample or the reaction progress, the oxidized areas generally have [110]-trending boundaries.

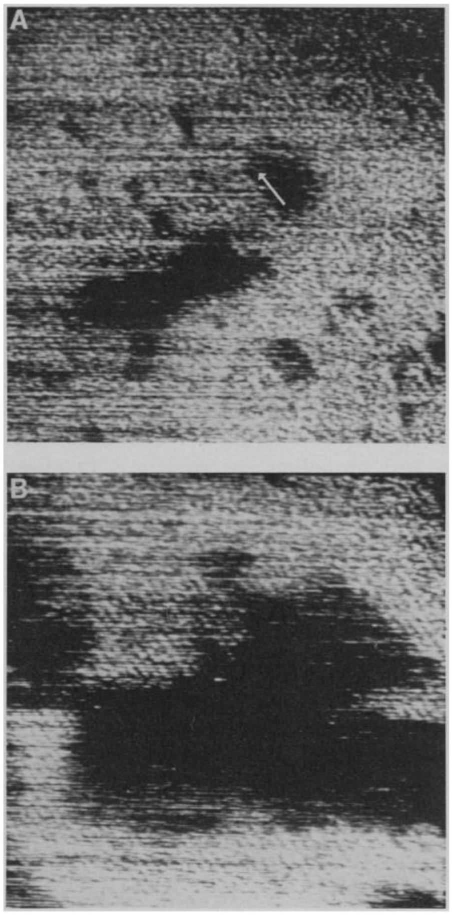

Fig. 1. (**A**) Galena imaged in air within 3 min of cleavage. Dominant spots, most likely corresponding to S sites (*9*), can be discerned. Dark sites and areas probably result from S oxidation. Arrow points along [110]. Image size is 22 by 22 nm. (**B**) The area shown in (A) after the next scan was completed (33 s later). The oxidized areas have expanded and coalesced. The apparent horizontal reaction fronts are along the direction of the scan and probably directly tip-induced or an artifact of limited time resolution. Both images were taken in a constant current mode with a tungsten tip, a tip bias of −200 mV, and a tunneling current of 1 nA.

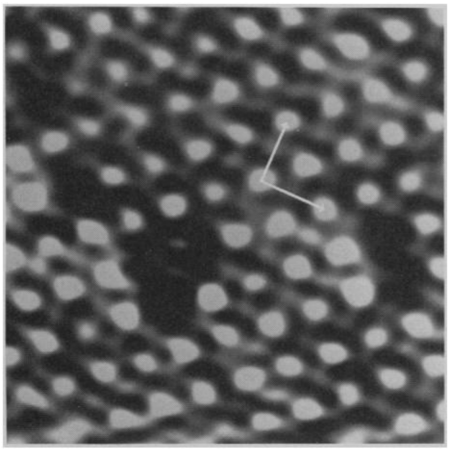

Fig. 2. High-resolution STM image taken with the tip and sample under oil (*13*) to exclude air, after the sample had been immersed in deionized water for 1 min immediately after cleavage. The dominant spots are assigned to S sites, and the weak spots between are assigned to Pb sites (*9*). The arrows outline a surface unit cell. The apparent vacancies probably correspond to oxidized S sites, similar to the small dark areas in Fig. 1A. Image size is 4.2 by 4.2 nm, collected at a tip bias of −200 mV and a tunneling current of 1.8 nA in constant height mode.

The oxidation reaction imaged in Fig. 1 occurred mainly under the area being scanned by the STM tip. For example, after following the reaction to completion in one area, we could move to a new area to find that the reaction was in an earlier stage of progress. Most likely, oxidation was accelerated only in the immediate vicinity of the tip. Other areas of the sample probably oxidized at the much slower rate characteristic of galena in air (*10*). To confirm that the dark areas resulted from reaction with air and not solely from scanning influences, we imaged a fresh galena surface under oil (*13*). Dark areas were rare and grew over hours instead of minutes, a rate probably limited by the diffusion of air through the oil. Moreover, when we exposed a fresh cleavage surface to water for 1 min and then imaged this surface under oil, small oxidized patches were common (Fig. 2) and stable during imaging; this observation suggests that oxidation occurred during water exposure.

In these experiments (Figs. 1 and 2), oxidized areas appeared to nucleate and grow rather than form by random oxidation of individual S sites. This observation implies that oxidized surface S (S_{ox}) exerted an influence on neighboring unoxidized surface S (S_{unox}), making the unoxidized sites more susceptible to oxidation. Such an influence, perhaps in the form of an altered local potential for S_{unox} with nearest neighbor S_{ox}, would help explain why oxidized areas were bounded by [110]-trending reaction fronts. S_{unox} on a [100] reaction front has two S_{ox} nearest neighbors and thus might oxidize more readily than S_{unox} on a [110] front where there is only one S_{ox} nearest neighbor. This process may allow faster advance of [100] fronts relative to [110] fronts; fast-moving fronts obliterate themselves relative to slow-moving fronts, analogous to crystal growth. Established [110] fronts may most efficiently advance, one row

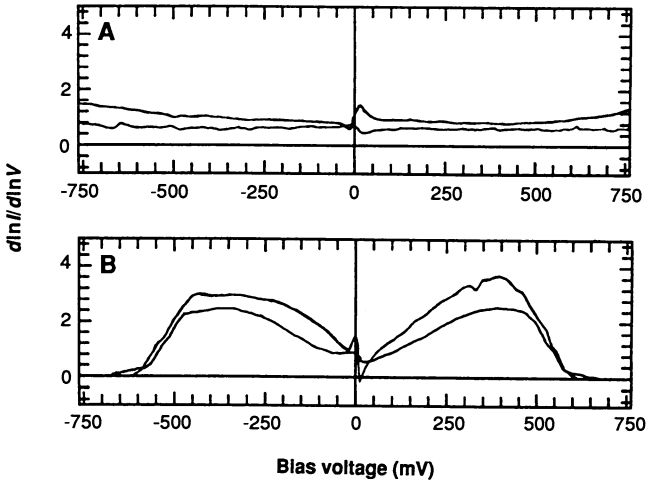

Fig. 3. (**A**) Spatially averaged *d*ln*I*/*d*ln*V* spectrum taken over the area imaged in Fig. 5A (upper curve) together with a similar spectrum taken over an Au metal film on mica (lower curve). (**B**) Spatially averaged *d*ln*I*/*d*ln*V* spectrum taken over the area imaged in Fig. 5B (upper curve), together with a similar spectrum taken over air-oxidized galena (lower curve). Cutoff of spectra for galena at higher voltage is an artifact of current amplifier saturation.

at a time, by kink migration along the front (kink sites on [110] fronts have two S_{ox} nearest neighbors). However, our time resolution was insufficient to follow kink motion in air.

For Au sorption studies, fresh galena surfaces were immersed in 1 ppm Au(III) (added as $KAuCl_4$), 1.1 M NaCl, pH = 3.2 (adjusted with HCl) solution at 25°C for various times (1 min to several hours; $AuCl_4^-$ is the stable gold complex in this solution). Under similar conditions, it has been shown by PES (*14*) that Au is sorbed onto the sulfide surface and reduced to Au(0) and that Cl^- does not adsorb to the galena surface. After reaction, samples were removed, rinsed briefly in deionized water, and wick-dried. The samples were imaged under oil to suppress reaction with air.

Positive identification of Au sorbed on galena was performed with the use of $d\ln I/d\ln V$ tunneling spectroscopy in air, where I is the tunneling current and V is the applied bias voltage (Fig. 3) (*15*). The spectra show that Au has a uniform density of states near the Fermi level (E_F), whereas galena has increasing density of states away from E_F; these spectral features are qualitatively similar to those obtained for Au on GaAs(110) surfaces in vacuum (*16*). Spectra collected from Au islands and exposed galena were consistently similar to those shown in Fig. 3 and could be used to distinguish between the two materials.

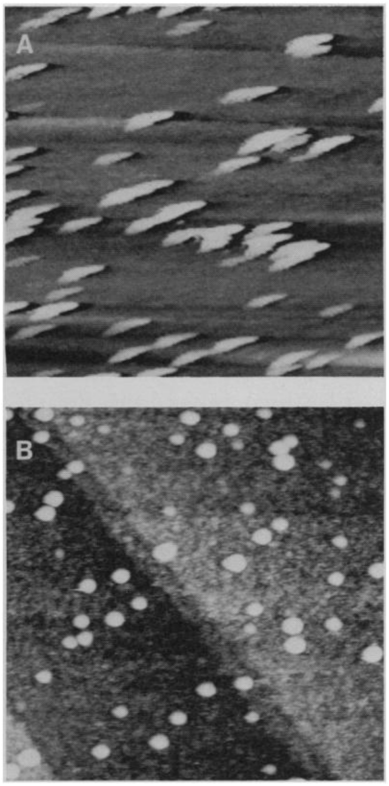

Fig. 4. Gold islands formed on a fresh (**A**) and preoxidized (**B**) galena (100) cleavage surface after exposure for 1.5 hours to the Au-bearing solution (see text). Image size is 800 by 800 nm in (A) and 275 by 275 nm in (B). Both images were collected at a tip bias of −200 mV and a tunneling current of 0.85 nA in constant current mode.

Islands of metallic Au that formed on the galena surface after 1.5 hours of exposure to the Au-bearing solution are shown in Fig. 4A. These islands were 100 ± 20 nm long, 10 ± 2 nm wide, and 6 ± 1 nm high and were not preferentially associated with [100]-trending steps. The islands grew along only two of the four crystallographically equivalent [110] directions on this surface, even after exposure for up to 2 days. This may be related to the fact that we used cleaved surfaces in these experiments. It has been suggested (*6*) that edge dislocations form on galena cleavage surfaces with orientations that are dependent on the direction of breakage. Oriented, cleavage-induced defects, if present, may help promote island growth in certain directions and not in other crystallographically equivalent directions (for example, see Fig. 5B). We repeated the 1.5-hour experiment using preoxidized galena (*3*); the surface (Fig. 4B) appeared rough and pitted, as previously found for oxidized surfaces (*8*). Gold islands were hemispherical, not elongated. The preoxidized surface was less reactive; the fresh surface sorbed the equivalent of 7 ± 1 monolayers of Au in 1.5 hours, compared to 2.5 ± 0.5 monolayers for the preoxidized surface, at least within these and other imaged areas. These results are in qualitative agreement with earlier PES results (*14*).

Gold islands on fresh galena surfaces and neighboring exposed galena were imaged at atomic resolution in air to see if structural registry considerations might explain Au island elongation (Fig. 5, A and B). On Au islands, a hexagonal array with a spacing of 0.5 ± 0.1 nm was observed; this pattern and spacing do not correspond with the most common growth surface for Au, a (111) face, where the atoms are in a closest packed arrangement with a spacing of 0.29 nm. However, it does correspond with a $\sqrt{3}$ by $\sqrt{3}$ overlayer on Au(111). In other cases in which we obtained atomic resolution of adsorbed Au, a $\sqrt{3}$ by $\sqrt{3}$ pattern was always observed but never in ordered domains larger than about 10 nm in diameter. A $\sqrt{3}$ by $\sqrt{3}$R30° structure has been observed in situ for the first layer of Cu coadsorbed to Au(111) with other molecules (*17*), and we speculate that $AuCl_4^-$ anions might behave similarly as they sorb to Au surfaces; however, this leaves important questions about the mechanistic role of the $\sqrt{3}$ by $\sqrt{3}$ overlayer on a growing Au particle.

One of the three equivalent directions of closest atomic spacing on the $\sqrt{3}$ by $\sqrt{3}$ structure (marked A–A′ in Fig. 5A) is aligned with the [010] direction of the galena substrate (Fig. 5B). Similar orientations with either the galena [100] or [010] directions were observed for other $\sqrt{3}$ by $\sqrt{3}$ Au domains. Although these data show that there is a tendency toward particular orientations of small ordered Au domains on growing Au islands on galena, it is not obvious why ordered Au domains should line up so as to produce elongation of Au islands along the galena [110] direction.

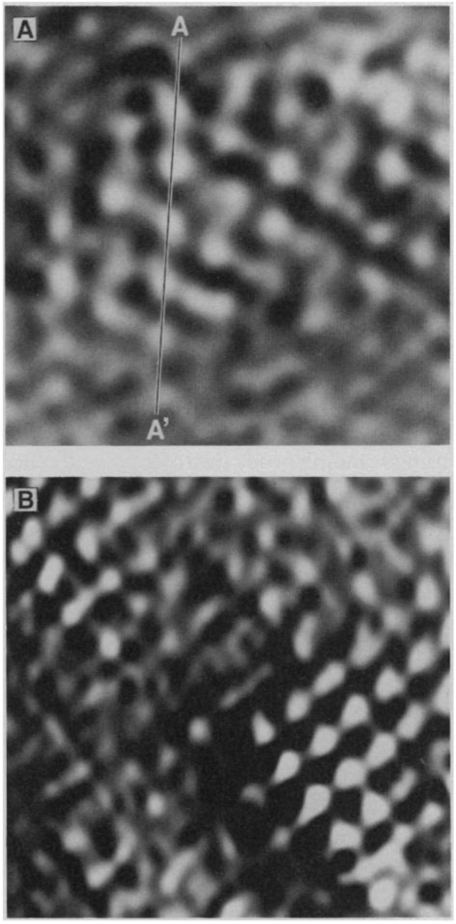

Fig. 5. (**A**) High-resolution STM image taken atop an Au island formed on a fresh PbS surface after 2 hours in an Au-bearing solution. The structure is a $\sqrt{3}$ by $\sqrt{3}$ pattern relative to the unreconstructed Au(111) surface; spectra taken over this area are presented in Fig. 3A and confirm the Au composition. The imaged area is 3.8 by 3.8 nm, collected at a tip bias of −200 mV and a tunneling current of 3.2 nA in constant height mode. See text for explanation of A–A′. (**B**) High-resolution STM image taken to the side of the Au island imaged in (A) and exhibiting the spectrum presented in Fig. 3B. The arrangement of S sites on the galena (100) surface can be seen. Note the defect in this image (atomic rows are offset from upper left to lower right); such defects may play a role in preferred oreintation of oxidation fronts and Au islands. The imaged area is 5 by 5 nm, collected at a tip bias of +600 mV and a tunneling current of 4.7 nA in constant height mode.

On the other hand, the galena [110] direction is preferred by oxidation reaction fronts (Figs. 1 and 2), and a direct coupling of the sorption and reduction of aqueous Au with the initial oxidation of surface sulfide sites could produce the nucleation and growth of small Au clusters in this direction. We propose that such clusters grow and coalesce to form ordered domains within [110]-trending Au islands, as observed. It is likely that Au islands also grow by the diffusion of reduced Au along the galena surface to growing Au clusters. In either case, Au reduction is probably accompanied by polysulfide (S_x^{2-}) formation and Pb release into solution, with eventual formation and release of SO_4^{2-} (*18*). On preoxidized surfaces, similar mechanisms produce Au islands, except that there is little to no direct Au deposition on unoxidized surface sites. Thus, the oxidized galena surface exerts little influence on the shape and orientation of Au islands, and the rate of reaction is reduced by a factor of about 3.

We have extended previous studies of aqueous Au deposition on sulfides to show that surface oxidation, as well as oxidation-related Au deposition, are governed by surface structure to a degree that depends on the history of the surface. Further studies using scanning probe microscopes and other surface-sensitive techniques will add to our understanding of sulfide oxidation kinetics and mechanisms. Such knowledge will prove useful not only for understanding certain aspects of ore-forming processes, but it should also be applicable to ore-processing methods and to the environmental chemistry of sulfides.

REFERENCES AND NOTES

1. B. M. Bakken, M. F. Hochella, Jr., A. F. Marshall, A. M. Turner, *Econ. Geol.* **84**, 171 (1989); B. M. Bakken, thesis, Stanford University (1990).
2. G. M. Bancroft and M. M. Hyland, in *Mineral-Water Interface Geochemistry, Reviews in Mineralogy 23*, M. F. Hochella, Jr., and A. F. White, Eds. (Mineralogical Society of America, Washington, DC, 1990), chap. 13; A. Starling, J. M. Gilligan, A. H. C. Carter, R. P. Foster, R. A. Saunders, *Nature* **340**, 298 (1989).
3. STM imaging and spectroscopy were accomplished with the use of a Digital Instruments Nanoscope II equipped with an electrically isolated sample stage and tungsten tips etched in 1 M KOH. All surfaces used in this study were galena (100) cleavage planes exposed by fracture in air and either used immediately or allowed to age in air for several months (the latter are referred to as preoxidized surfaces). Galena has the NaCl structure and a bulk band gap of 0.4 eV, although the surface band gap is probably considerably less.
4. J. A. Tossell and D. J. Vaughn, *Can. Mineral.* **25**, 381 (1987).
5. M. F. Hochella Jr., *et al.*, *Am. Mineral.* **74**, 1233 (1989); M. F. Hochella, Jr., in *Mineral-Water Interface Geochemistry, Reviews in Mineralogy 23*, M. F. Hochella, Jr., and A. F. White, Eds. (Mineralogical Society of America, Washington, DC, 1990), chap. 3.
6. N. J. Zheng *et al.*, *Phys. Rev. B* **38**, 12780 (1988).
7. I. H. Wilson, N. J. Zheng, U. Knipping, I. S. T. Tsong, *Appl. Phys. Lett.* **53**, 2039 (1988); T. G. Sharp, N. J. Zheng, I. S. T. Tsong, P. R. Buseck, *Am. Mineral.* **75**, 1438 (1990).
8. G. F. Cotterill, R. Bartlett, A. E. Hughes, B. A. Sexton, *Surf. Sci. Lett.* **232**, L211 (1990).
9. C. M. Eggleston and M. F. Hochella, Jr., *Geochim. Cosmochim. Acta* **54**, 1511 (1990).
10. A. N. Buckley and R. Woods, *Appl. Surf. Sci.* **17**, 401 (1984).
11. J. R. Gardner and R. Woods, *J. Electroanal. Chem.* **100**, 447 (1979).
12. PES shows evidence for chemisorption of O species (O_2, OH^-, H_2O, CO_2) within 1 min of exposure to air or water but no detectable sulfide oxidation for up to a day in air (*10*).
13. We use polyphenyl ether, a nonpolar, high molecular weight oil that has been utilized in other STM studies (*9*) and is not seen in STM images.
14. G. E. Jean and G. M. Bancroft, *Geochim. Cosmochim. Acta* **49**, 979 (1985).
15. For $d\ln I/d\ln V$ spectroscopy, 10 to 50 spectra were averaged and the feedback loop was run for 300 μs between individual spectra collections to stabilize the tip-sample separation. Tip stabilization was crucial to avoid tip crashes during data collection.
16. R. M. Feenstra, *J. Vac Sci. Technol. B* 7, 925 (1989).
17. O. M. Magnussen, J. Hotlos, R. J. Nichols, D. M. Kolb, R. J. Behm, *Phys. Rev. Lett.* **64**, 2929 (1990); S. Manne, P. K. Hansma, J. Massie, V. B. Elings, A. A. Gewirth, *Science* **251**, 183 (1991).
18. M. M. Hyland and G. M. Bancroft, *Geochim. Cosmochim. Acta* **53**, 367 (1989).
19. We thank B. Bakken, G. Brown, G. Parks, V. Elings, J. Peck, C. Lang, S. Strauss, S. Stipp, P. Johnsson, and D. Coulman for helpful discussions, assistance, or materials. The Center for Materials Research at Stanford University provided financial and instrumental support. This work was also supported by grants from the Petroleum Research Fund (administered by the American Chemical Society) and the National Science Foundation (grants PRF 22892-AC5,2 and EAR-9105000, respectively, both to M.F.H.).

13 May 1991; accepted 13 August 1991

Hydrogen-Helium Mixtures at Megabar Pressures: Implications for Jupiter and Saturn

J. E. KLEPEIS,* K. J. SCHAFER, T. W. BARBEE III, M. ROSS

Models of Jupiter and Saturn postulate a central rock core surrounded by a fluid mixture of hydrogen and helium. These models suggest that the mixture is undergoing phase separation in Saturn but not Jupiter. State-of-the-art total energy calculations of the enthalpy of mixing for ordered alloys of hydrogen and helium confirm that at least partial phase separation has occurred in Saturn and predict that this process has also begun in Jupiter.

PLANETARY MODELS ARE CONSTRUCTED on the basis of observed characteristics such as the total mass, radius, rotation rate, and gravitational field of the planet. These measured quantities plus observations of the planetary atmospheres of Jupiter and Saturn are consistent with a hydrogen-helium mixture composed of 7% helium by number (23% by weight, the solar abundance) surrounding a central rock core (*1*). On the basis of these inputs, planetary evolution models can be used to determine the thermodynamic conditions as a function of time in the interior of the planet. The maximum temperature and pressure in the mixture occurs at the central core boundary; the best estimates for the current values are 45 Mbar and 20,000 K for Jupiter and 10 Mbar and 10,000 K for Saturn (*1*).

Evolutionary models also can be used to determine the energy output of the planet as a function of time. These models yield a cooling rate for Jupiter that is consistent with both its measured energy output and the approximate age of the solar system, but the corresponding rate for Saturn is too fast (*1–3*). It has been suggested (*4*) that, as the planets cooled, a temperature might have been reached at some distance from the central core at which helium-rich droplets would condense out of the hydrogen-helium mixture (phase-separate), releasing gravitational energy as they settled. This extra source of energy might then account for the anomalously slow cooling of Saturn. However, it has been assumed that this process has not occurred in Jupiter (*1, 2*). Thus far, the only internal energy source included in evolutionary models is the heat generated as a result of the gravitational collapse that occurred during the formation of the planet (*1*). Calculations including the possibility of phase separation have yet to be carried out [Stevenson and Salpeter (*2*) have discussed the detailed implications of phase separation but in general terms only]. A crucial ingredient in these calculations will be the pressure and temperature dependence of the miscibility gap in the hydrogen-helium mixture. In the calculations presented here we use state-of-the-art total energy (TE) methods to address this question.

At the pressures in the interiors of Jupiter and Saturn, hydrogen is believed to be a liquid metal (*5*) whereas helium should be

---

University of California, Lawrence Livermore National Laboratory, Livermore, CA 94550.

*To whom correspondence should be addressed.